Journal of Alloys and Compounds 595 (2014) 80–86

Contents lists available at ScienceDirect

Journal of Alloys and Compounds

journal homepage: www.elsevier.com/locate/jalcom

# Mechanical properties and electronic structure of anti-$ReO_3$ structured cubic nitrides, $M_3N$, of d block transition metals M: An *ab initio* study

Xiuquan Zhou [a], Daniel Gall [b], Sanjay V. Khare [c,*]

[a] Department of Chemistry, The University of Toledo, 2801 West Bancroft Street, Toledo, OH 43606, United States
[b] Department of Materials Science and Engineering, Rensselaer Polytechnic Institute, 110 8th Street, Troy, NY 12180, United States
[c] Department of Physics and Astronomy, The University of Toledo, 2801 West Bancroft Street, Toledo, OH 43606, United States

ARTICLE INFO

*Article history:*
Received 21 September 2013
Received in revised form 14 January 2014
Accepted 16 January 2014
Available online 27 January 2014

*Keywords:*
*Ab initio* calculations
Elastic constants
Anti rhenium trioxide structure
Transition metal nitrides
Hardness

ABSTRACT

We report a systematic study of the anti-$ReO_3$ structured transition metal nitrides, $M_3N$, using *ab initio* density functional theory computations in the local density approximation. Here M denotes all the 3*d*, 4*d* and 5*d* transition metals. Our calculations indicate that all $M_3N$ compounds except $V_3N$ of group 5 and $Zn_3N$ and $Hg_3N$ of group 12 are mechanically stable. For the stable $M_3N$ compounds, we report a database of predictions for their lattice constants, electronic properties and mechanical properties including bulk modulus, Young's modulus, shear modulus, ductility, hardness and Debye temperature. It is found that most $M_3N$ compounds exhibit ductility with Vickers hardness between 0.4 GPa and 11.2 GPa. Our computed lattice constant for $Cu_3N$, the only $M_3N$ compound where experiments exist, agrees well with the experimentally reported values. We report ratios of the melting points of all $M_3N$ compounds to that of $Cu_3N$. The local density of states for all $M_3N$ compounds are obtained, and electronic band gaps are observed only for M of group 11 (Cu, Ag and Au) while the remaining $M_3N$ compounds are metallic without band gaps. Valence electron density along with the hybridization of the metal *d* and nitrogen 2*p* orbitals play an important role in determining the stability and hardness of different compounds. Our high-throughput databases for the cubic anti-$ReO_3$ structured transition metal nitrides should motivate future experimental work and shorten the time to their discovery.



## 1. Introduction

Transition metal nitrides (TMNs) have been suitable coating materials, especially for hard coatings, for their excellent mechanical, anti-wear, optical, electrical and magnetic properties [1–6]. In order to search for super hard materials, novel TMNs with outstanding hardness have been synthesized experimentally, such as novel platinum nitride, osmium nitride and iridium nitride prepared at high pressures using laser heated diamond anvil cells [7,8]. Theoretical investigations can help with the structure determination when pure experimentally derived conclusions are challenging to make [9–12]. Furthermore, theoretical calculations can facilitate the discovery of novel super hard TMNs and focus experimental attention to likely material choices for obtaining desired physical properties. This is particularly true for high-throughput computations which can rapidly span across regions of the periodic table saving considerable experimental effort and expense and accelerating time to discovery [2,13,14]. In addition, the high-throughput materials databases created by systematic theoretical studies can provide valuable information for deriving semi-empirical models that yield relationships between material properties. In the quest for exploring binary TMNs using first-principle calculations, studies have been focused on TMNs with nitrogen to metal ratios of 1:1 assuming the rocksalt, zinc blende, and cesium chloride structures and 2:1 assuming the fluorite and pyrite structures [11,13–18]. The tendency for such TMNs to be stable across a large range of metal to nitrogen ratios is well known, resulting in many different phases. Thus to create a comprehensive materials database, for binary TMNs, studies on other compositions are also required. This manuscript is a step towards creating such a database for TMNs of cubic symmetry.

Choice of a structure and composition was motivated by the anti-$ReO_3$ structured copper nitride, $Cu_3N$, first synthesized by Juza and Hahn [19] in 1938 by the reaction of $CuF_2$ and $NH_3$ at 553 K. Later, Zachwieja and Jacobs [20] obtained $Cu_3N$ single crystals using copper complexes and liquid ammonia. Recently, $Cu_3N$ has been extensively studied both experimentally and theoretically for its promising optical and electrical properties [6,21–24]. Inspired by previous studies on $Cu_3N$, here we report a first-principles

* Corresponding author. Tel.: +1 419 530 2292.
*E-mail address:* sanjay.khare@utoledo.edu (S.V. Khare).

http://dx.doi.org/10.1016/j.jallcom.2014.01.116
0925-8388/

investigation on $M_3N$ (M stands for transition metals of the fourth, fifth and sixth periods except for lanthanides) compounds with the anti-$ReO_3$ structure. Except for $Cu_3N$, there appear to be no theoretical or experimental reports in the literature on the remaining 29 $M_3N$ compounds. In the present work, lattice constants, stability, mechanical properties including elastic constants, multi-crystalline elastic moduli, hardness and Debye temperature and electronic properties of $M_3N$ compounds are obtained using *ab initio* calculations. This systematic investigation should spur more experimental work on these $M_3N$ compounds.

## 2. Computational method

All the *ab initio* calculations in this work were performed by using the Vienna *Ab-initio* Simulation Package (VASP) [25–27] codes within the local density approximation (LDA) to density functional theory (DFT) [28,29]. The electron–ion interactions were treated by ultrasoft-Vanderbilt type pseudo potentials [30] as supplied by Kresse and Hafner [31]. A cutoff energy of 400 eV, was applied to the valence electron wave functions expanded in a plane-wave basis set for all the $M_3N$ (M is any transition metal of period IV, V and VI) compounds. A Monkhorst–Pack [32] generated, $12 \times 12 \times 12$ *k*-point grid was used for the Brillouin-zone integrations in all calculations except for calculations of local density of states (LDOS), where a $24 \times 24 \times 24$ *k*-point grid was used. Tests using cutoff energies and k-points mentioned above reached a convergence better than 1 meV. The minimum energy for each $M_3N$ compound was obtained by fully relaxing all atoms and lattice constants until a force convergence better than 0.01 eV/Å was achieved.

The equilibrium lattice constant ($a$) was obtained by second order polynomial fitting of total energy as a function of volume, where the equilibrium volume ($V$) was corresponding to the minimum energy. For each optimized compound, three different external strain tensors ($\bar{\epsilon}$) as described by Mehl et al. [33] and Patil et al. [11,13] with the values of the strain component $\delta$ of ±1%,±2%,±3% and ±4% were applied to its equilibrium primitive cell, while allowing full relaxation of the ions, to calculate the three independent elastic constants, $C_{11}$, $C_{12}$, and $C_{44}$, of cubic crystal systems. In order for the cubic structure to be mechanically stable, the following criteria have to be satisfied [34]:

$$(C_{11} - C_{12}) > 0, \quad (C_{11} + 2C_{12}) > 0, \quad C_{11} > 0, \quad C_{12} > 0, \quad C_{44} > 0. \tag{1}$$

For materials with cubic structures, the equilibrium bulk modulus ($B$) is related to the elastic constants by the relation, $B = (C_{11} + 2C_{12})/3$. Different methods may give different values, but the results remain fairly invariant under change of computational model. For bulk modulus, the results obtained using this method are only slightly different from other equations of state, such as Birch–Murnaghan [35,36], Poirier–Tarantola [37] and Anton–Schmidt [38] models. Values obtained using these three models for $Cu_3N$ are 146.8 GPa, 147.0 GPa and 147.6 GPa, respectively. These values are within 1% of our value 147.9 GPa obtained by the equation $B = (C_{11} + 2C_{12})/3$.

## 3. Results and discussion

### 3.1. Lattice and elastic constants

The anti-$ReO_3$ structured $M_3N$ compounds (space group $Pm\bar{3}m$), are made of nitrogen atoms occupying the corners of the primitive cubic cell and metal atoms occupying all the centers of the 12 edges of the cubic cell. This structure can be considered as N atoms occupying the octahedral interstices (6-coordinated) of the cubic close packed arrangement of metal atoms with 1/4 of the metal sites vacant. The orthogonal lattice vectors of the unit cell are given by $\vec{\mathbf{a}}_1 = a(1, 0, 0)$, $\vec{\mathbf{a}}_2 = a(0, 1, 0)$ and $\vec{\mathbf{a}}_3 = a(0, 0, 1)$, where $a$ is the equilibrium lattice constant. The basis atoms in direct terms of the lattice vectors are located at $\mathbf{b}_{M1} = 1/2\,\vec{\mathbf{a}}_1$, $\mathbf{b}_{M2} = 1/2\,\vec{\mathbf{a}}_2$, $\mathbf{b}_{M3} = 1/2\vec{\mathbf{a}}_3$ and $\mathbf{b}_N = (0, 0, 0)$, where M and N denote metal and nitrogen atoms, respectively. We computed equilibrium lattice constants ($a$), the three independent elastic constants $C_{11}$, $C_{12}$ and $C_{44}$, and bulk modulus of this anti-$ReO_3$ cubic structure of $M_3N$ compounds. These are shown in Table 1. For each period, the calculated lattice constants initially decrease with the increase of group number until group 8, and increase thereafter. Compared to the literature, the calculated lattice constant of $Cu_3N$ (3.742 Å) is about 1.7–2.0% smaller than previous experimental values, 3.807 Å, 3.819 Å, and 3.817 Å for initial discovery in 1938 [19], single crystal X-ray diffraction [20], and synchrotron powder X-ray diffraction [22], respectively. Other *ab initio* calculations of $Cu_3N$ reported lattice constants of 3.752 Å for LDA, and 3.868 Å and 3.83 Å for GGA [39,40]. Our result for $Cu_3N$ is in good agreement with values in the literature. For the remaining $M_3N$ compounds, previous experimental or theoretical data are not available. Our results indicate that all $M_3N$ compounds are energetically stable, and for each row, the cohesive energies initially increase with the increase of group number until group 6, and decrease thereafter. In addition, it is found that the cohesive energies of $M_3N$ compounds decrease significantly for group 11 (Cu, Ag and Au) and 12 (Zn, Cd and Hg). Hence, $M_3N$ compounds of group 3–10 possess larger cohesive energies than $Cu_3N$. This makes them energetically more stable than $Cu_3N$ which has been synthesized experimentally [5,19–21]. Furthermore, these experiments have shown it to be stable up to a temperature of about 740 K. Our work can thus motivate the discovery of the other $M_3N$ compounds.

**Table 1**
Lattice constant a (Å), elastic constants, $B$, $C_{11}$, $C_{12}$ and $C_{44}$ (GPa) of nitrides, $M_3N$, of period IV, V and VI transition metals M. Values for compounds that were found to be unstable are denoted by the symbol "U".

| Elements | | | Atomic number | | | Lattice constant (Å) | | | $B$ (GPa) | | |
|---|---|---|---|---|---|---|---|---|---|---|---|
| Sc | Y | N/A | 21 | 39 | N/A | 4.484 | 4.872 | N/A | 66.3 | 71.1 | N/A |
| Ti | Zr | Hf | 22 | 40 | 72 | 4.103 | 4.502 | 4.389 | 145.6 | 128.3 | 144.6 |
| V | Nb | Ta | 23 | 41 | 73 | 3.874 | 4.258 | 4.201 | 199.0 | 187.4 | 211.8 |
| Cr | Mo | W | 24 | 42 | 74 | 3.720 | 4.089 | 4.067 | 229.2 | 222.0 | 268.4 |
| Mn | Tc | Re | 25 | 43 | 75 | 3.653 | 3.971 | 3.993 | 258.6 | 253.9 | 298.5 |
| Fe | Ru | Os | 26 | 44 | 76 | 3.608 | 3.942 | 3.971 | 245.0 | 247.6 | 293.4 |
| Co | Rh | Ir | 27 | 45 | 77 | 3.610 | 3.972 | 4.016 | 228.1 | 219.1 | 264.1 |
| Ni | Pd | Pt | 28 | 46 | 78 | 3.650 | 4.048 | 4.103 | 199.3 | 168.3 | 205.7 |
| Cu | Ag | Au | 29 | 47 | 79 | 3.775 | 4.249 | 4.287 | 147.9 | 102.2 | 129.5 |
| Zn | Cd | Hg | 30 | 48 | 80 | 4.054 | 4.530 | 4.670 | 80.6 | 64.1 | 40.7 |

| $C_{11}$ (GPa) | | | $C_{12}$ (GPa) | | | $C_{44}$ (GPa) | | |
|---|---|---|---|---|---|---|---|---|
| 131.6 | 124.8 | N/A | 33.7 | 44.3 | N/A | 9.3 | 10.4 | N/A |
| 280.8 | 233.6 | 272.0 | 78.0 | 75.6 | 80.9 | 24.0 | 21.9 | 27.1 |
| 344.2 | 315.9 | 346.0 | 126.4 | 123.1 | 144.7 | U | 16.9 | 6.1 |
| 503.0 | 489.0 | 565.9 | 92.3 | 88.5 | 119.7 | 27.1 | 36.0 | 60.7 |
| 618.8 | 567.7 | 667.1 | 78.6 | 97.0 | 114.2 | 28.5 | 15.2 | 51.4 |
| 558.1 | 527.7 | 603.9 | 88.5 | 107.5 | 138.1 | 46.2 | 54.0 | 60.8 |
| 485.1 | 426.1 | 495.2 | 99.6 | 115.7 | 148.5 | 57.4 | 61.3 | 82.7 |
| 399.1 | 298.2 | 340.8 | 99.4 | 103.3 | 138.2 | 38.3 | 31.3 | 17.2 |
| 311.5 | 202.2 | 229.9 | 66.2 | 52.3 | 79.2 | 18.5 | 12.7 | 10.8 |
| 118.7 | 102.4 | 49.8 | 61.6 | 44.9 | 36.1 | U | 0.4 | U |

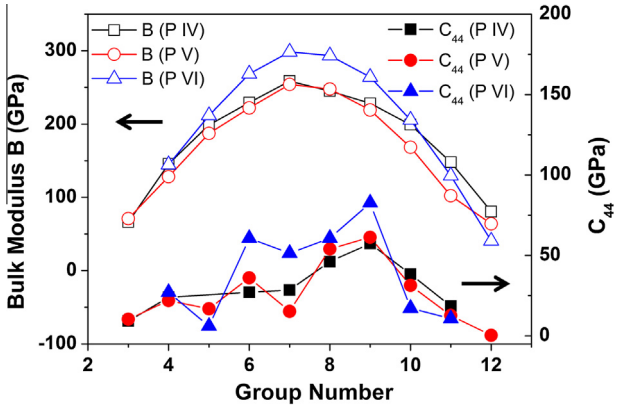


**Fig. 1.** Bulk moduli ($B$), left axis open symbols, and elastic constant $C_{44}$, right axis closed symbols, of transition metal nitrides $M_3N$ as a function of group number of the metal (M). Square, circle and triangle represent data for periods IV, V and VI of M, respectively. For example, values for group number 4 correspond to $Ti_3N$, $Zr_3N$ and $Hf_3N$.

The trend for variation of the bulk modulus ($B$) with group and column number is clear from Fig. 1. Values of $B$ increase with group number and peak at group 7 for each period, and increase with the increase of atomic number for each column except for group 11 and 12. Similar trends are seen for values of $C_{11}$ from Table 1. Variations in $C_{12}$ and $C_{44}$ with group and column numbers are similar to each other, but not as smooth as those for bulk modulus and $C_{11}$. No clear trend with the change in period number, from 4 to 6, is seen in Fig. 1. For $C_{44}$, an indicator of the stability against shear deformation and hardness as described in literature [2,41–43], the largest value for each period occurs for group 9 transition metal nitrides $Co_3N$, $Rh_3N$ and $Ir_3N$ with values of 57.4, 61.3 and 82.7 GPa respectively. We observe that the average number of valence electrons per atom, also called the valence electron density (VED), for group 9 $M_3N$ compounds is 8, a number associated with closed shell electronic configurations for noble gas atoms as well as a magic number for metal clusters [44]. Similar to our result, a nearby value, VED of about 8.4, was found to be related to the highest values of $C_{44}$ value for transition metal carbonitrides and nonstoichiometric nitrides, such as $TiC_xN_{1-x}$ and $TiN_{1-x}$ of the rocksalt structure [1,2]. Patil et al. [13] found a maximum in $B$ for pyrite phases of period six transition metal nitrides near a VED of 18, another value equaling closed shell number of electrons in atoms.

Although all calculated $M_3N$ compounds are energetically stable, $V_3N$, $Zn_3N$ and $Hg_3N$, which are denoted as "U" in Table 1, are mechanically unstable because of negative $C_{44}$ values. All other transition metal $M_3N$ compounds are mechanically stable, and therefore their experimental synthesis is expected to be possible.

### 3.2. Mechanical properties

The effective medium shear modulus ($G$) and Young's modulus ($E$) can be obtained using Hill's approximation [45], as the true values lie between Voigt's [46] (upper limit) and Reuss's [47] (lower limit) approximation:

$$G_H = 1/2\,(G_V + G_R). \quad (2)$$

and

$$E_H = 1/2\,(E_V + E_R). \quad (3)$$

The subscripts H, V and R denote elastic moduli obtained using Hill's, Voigt's and Reuss's approximation, respectively. For cubic crystal systems, shear modulus ($G$) can be calculated from the three independent elastic constants, $C_{11}$, $C_{12}$ and $C_{44}$ using a well known result also described by Chung and Buessem [48]:

$$G_V = [(C_{11} - C_{12}) + 3C_{44}]/5 \quad (4)$$

and

$$G_R = [5(C_{11} - C_{12}) \times C_{44}]/(4C_{44} + 3C_{11} - 3C_{12}). \quad (5)$$

Young's modulus can be calculated from bulk modulus ($B$) and shear modulus using the following equation:

$$E_H = 9B_HG_H/(3B_H + G_H). \quad (6)$$

From the three elastic moduli, $B$, $G$ and $E$, a variety of mechanical properties can be calculated, such as the Poisson's ratio [45] ($v$) and Pugh's ratio [49] ($k$) as $v = (3B - 2G)/[2(3B + G)]$ and $k = G/B$. Our calculations for $G_H$, $E_H$, $v$ and $k$ are given in Table 2. For each period, both Young's modulus ($E_H$), stiffness of a material ($B_H$), and shear modulus ($G_H$), the ability to resist shear strain, peak at group 8 or 9 (Table 2). Maximum $E_H$ and $G_H$ are observed for $Ir_3N$ with values of 294–112 GPa respectively, comparable to the rocksalt structured NbN [42]. Fig. 2 shows a comparison between $v$ and $k$, each of which indicates whether a material is likely to be ductile or brittle. Typical Poisson's ratio, values of $v$ for covalent, ionic, and metallic materials are 0.1, 0.25 and 0.33, respectively [50]. Higher values of $v$ indicate higher metallic behavior, and for metallic materials with $v$ above 0.33, higher $v$ values also indicate higher ductility [50]. Except for the unstable ones, all calculated Poisson's ratios for the $M_3N$ compounds are greater than 0.3 (Fig. 2), indicating more metallic behavior. Analogous to $v$, Pugh's ratio $k$ gives a measure of a material to be ductile [49]. It is known that $k \approx 0.57$ show borderline ductile behavior and materials of similar structures with lower $k$ values are more ductile. Therefore, $k$ is anticorrelated with $v$, which agrees with the reverse correlation between the two seen in Fig. 2. For all stable $M_3N$ compounds in Fig. 2, their Pugh's ratios are below 0.5, indicating some ductile behavior, which agrees with the calculated Poisson's ratios. Similar to $v$ and $k$, Cauchy pressure ($P_C \equiv C_{12} - C_{44}$) is also a good indicator of ductility of materials [51]. For cubic crystal systems, negative $P_C$

**Table 2**
Shear modulus, $G_H$ (GPa), Young's modulus, $E_H$ (GPa), Poisson's ratio, $v$, and Pugh's ratio, $k$ of nitrides, $M_3N$, of period IV, V and VI transition metals M. Values for compounds that were found to be unstable are denoted by the symbol "U".

| Elements | | | Atomic number | | | $G_H$ (GPa) | | | $E_H$ (GPa) | | | $v$ (Poisson's ratio) | | | $k$ (Pugh's ratio) | | |
|---|---|---|---|---|---|---|---|---|---|---|---|---|---|---|---|---|---|
| Sc | Y | N/A | 21 | 39 | N/A | 19 | 19 | N/A | 53 | 51 | N/A | 0.37 | 0.38 | N/A | 0.29 | 0.26 | N/A |
| Ti | Zr | Hf | 22 | 40 | 72 | 45 | 38 | 46 | 122 | 103 | 125 | 0.36 | 0.37 | 0.36 | 0.31 | 0.29 | 0.32 |
| V | Nb | Ta | 23 | 41 | 73 | U | 37 | 27 | U | 104 | 77 | U | 0.41 | 0.44 | U | 0.20 | 0.13 |
| Cr | Mo | W | 24 | 42 | 74 | 70 | 78 | 106 | 191 | 209 | 280 | 0.36 | 0.34 | 0.33 | 0.31 | 0.35 | 0.39 |
| Mn | Tc | Re | 25 | 43 | 75 | 85 | 64 | 109 | 229 | 177 | 291 | 0.35 | 0.38 | 0.34 | 0.33 | 0.25 | 0.36 |
| Fe | Ru | Os | 26 | 44 | 76 | 95 | 97 | 108 | 252 | 256 | 288 | 0.33 | 0.33 | 0.34 | 0.39 | 0.39 | 0.37 |
| Co | Rh | Ir | 27 | 45 | 77 | 96 | 90 | 112 | 252 | 237 | 294 | 0.32 | 0.32 | 0.31 | 0.42 | 0.41 | 0.42 |
| Ni | Pd | Pt | 28 | 46 | 78 | 69 | 50 | 38 | 185 | 137 | 108 | 0.35 | 0.36 | 0.41 | 0.35 | 0.30 | 0.19 |
| Cu | Ag | Au | 29 | 47 | 79 | 44 | 28 | 26 | 120 | 78 | 74 | 0.36 | 0.37 | 0.40 | 0.30 | 0.28 | 0.20 |
| Zn | Cd | Hg | 30 | 48 | 80 | U | 6 | U | U | 18 | U | U | 0.45 | U | U | 0.10 | U |

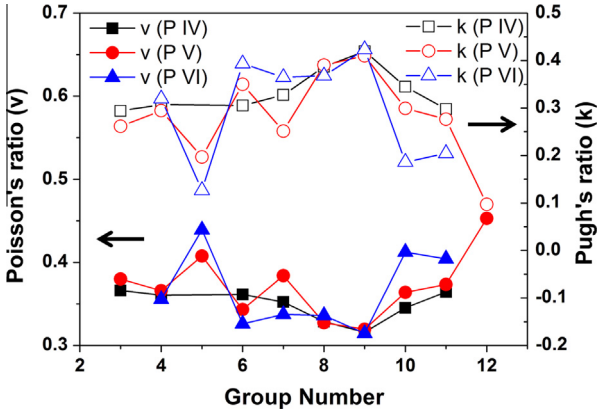


**Fig. 2.** Poisson's ratio ($v$), left axis closed symbols, and Pugh's ratio ($k$), right axis open symbols, of nitrides, $M_3N$, as a function of group number of the metal (M). Square, circle and triangle represent data for period IV, V and VI of M, respectively. For example, values for group number 5 correspond to $V_3N$, $Nb_3N$ and $Ta_3N$ while group number 12 correspond to $Zn_3N$, $Cd_3N$ and $Hg_3N$ compounds.

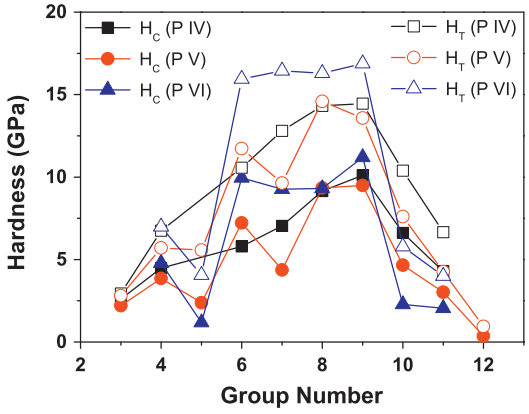


**Fig. 3.** Vickers hardness, Chen's model ($H_C$), closed symbols, and Teter's empirical model ($H_T$), open symbols, of nitrides, $M_3N$, as a function of group number of the metal (M). Square, circle and triangle represent data for $H_C$ ($H_T$) of period IV, V and VI of M, respectively. For example, values for group number 6 correspond to $Cr_3N$, $Mo_3N$ and $W_3N$ compounds.

indicates covalent (directional) bonding, while positive $P_C$ indicates metallic bonding [51]. In Table 1, all the $C_{44}$ values for stable $M_3N$ compounds are significantly smaller than those of $C_{12}$, indicating strong metallic bonding. This is consistent with the results for Poisson's and Pugh's ratios.

For many coating applications materials with high hardness are preferred. Hardness usually measured by Vickers hardness ($H_V$) has a long history of being theoretically modeled [2,41–43]. Teter [41] studied a variety of materials and proposed that $H_V$ is linearly correlated with shear modulus ($G$). The relation between Vickers hardness in Teter's form ($H_T$) and $G$ is described by Chen et al. [42] in the following equation:

$$H_T = 0.151\,G. \tag{7}$$

However, deviations from Eq. (7), were observed for many materials, as hardness is not only associated with shear modulus, but also the bulk modulus $B$, which was described by Chen et al. [42] as $H_C$ for which they provided a derivation from a physically motivated model yielding a relation:

$$H_C = 1.887\,k^{1.171}\,G^{0.591}. \tag{8}$$

Similar to the above relationship the Debye temperature ($\theta_D$) can be related to the elastic constants through the speed of sound as described by Anderson [52]:

$$\theta_D = \frac{h}{k_B}\left[\frac{3n}{4\pi}\left(\frac{N_A\rho}{M}\right)\right]^{1/3} v_m, \text{ where } v_m = \left[\frac{1}{3}\left(\frac{2}{v_t^3}+\frac{1}{v_l^3}\right)\right]^{-1/3}, \tag{9}$$

$$v_t = \left(\frac{G}{\rho}\right)^{1/2} \text{ and } v_l = \left(\frac{3B+4G}{3\rho}\right)^{1/2}. \tag{10}$$

Here $h$ is Planck's constant, $k_B$ is Boltzmann's constant, $N_A$ is Avogadro's number, $\rho$ is the mass density, M is the molar mass per unit cell, $n$ is the number of atoms per unit cell and $v_l$ and $v_t$ and $v_m$ are the longitudinal, transverse and mean sound speeds, respectively.

The calculated results for Vickers hardness, both $H_C$ and $H_T$, and the calculated Debye temperatures are given in Table 3. As shown in Fig. 3, both Chen's and Teter's model for Vickers hardness share a similar trend, except that the values of $H_T$ are about 5 GPa larger than those of $H_C$. Chen's model has provided a good statistical fit to experimentally measured Vicker's hardness of many different types of materials [42]. From Fig. 3 we observe that values of $H_C$ for the $M_3N$ compounds, with M = Co, Rh and Ir of group 9, M = Fe, Ru and Os of group 8 and M = W and Re of group 6 and 7 in the 6th period are significantly larger than the values for the remaining nitrides. With $H_C$ values between 9 and 11 GPa, the hardness of these $8M_3N$ compounds are comparable to steel and silicon with hardness of about 9–12 GPa, respectively [42,53]. The trend for hardness is very similar to that of $C_{44}$ (Figs. 1 and 3), and highest hardness is observed for group 9 $M_3N$ compounds with a VED of 8 with the highest hardness $H_C$ of 11.2 for $Pt_3N$.

Debye temperature ($\theta_D$) is related to hardness, as higher values of $\theta_D$ usually indicate higher inter-atomic binding forces, thus higher hardness [54]. For materials with the same crystal structure, the relationship between Debye temperature and hardness ($H_V$) can be described following Abrahams et al. [55] and Deus et al. [56] by the following equation:

$$\theta_D = m \times H_V^{1/2}\,\rho^{-1/6}\,M^{-1/3} + n, \tag{11}$$

**Table 3**
Vicker hardness (GPa), Chen's Model $H_C$, and Teter's empirical model $H_T$, Debye temperature (K), and ratio of melting temperature $T_m$ to the $T_m$ of $Cu_3N$ of nitrides, $M_3N$, of period IV, V and VI transition metals M. Values for compounds that were found to be unstable are marked by the symbol "U".

| Elements | | | Atomic number | | | $H_C$ (GPa) | | | $H_T$ (GPa) | | | Debye temperature (K) | | | $T_m/(T_m$ of $Cu_3N)$ | | |
|---|---|---|---|---|---|---|---|---|---|---|---|---|---|---|---|---|---|
| Sc | Y | N/A | 21 | 39 | N/A | 2.6 | 2.2 | N/A | 2.9 | 2.8 | N/A | 317 | 235 | N/A | 0.7 | 0.9 | N/A |
| Ti | Zr | Hf | 22 | 40 | 72 | 4.5 | 3.9 | 4.8 | 6.8 | 5.7 | 7.0 | 446 | 318 | 251 | 1.3 | 1.4 | 1.6 |
| V | Nb | Ta | 23 | 41 | 73 | U | 2.4 | 1.2 | U | 5.6 | 4.1 | U | 305 | 188 | U | 1.2 | 0.8 |
| Cr | Mo | W | 24 | 42 | 74 | 5.8 | 7.2 | 9.9 | 10.6 | 11.7 | 16.0 | 511 | 423 | 358 | 1.5 | 2.2 | 2.9 |
| Mn | Tc | Re | 25 | 43 | 75 | 7.0 | 4.4 | 9.3 | 12.8 | 9.6 | 16.4 | 543 | 376 | 359 | 1.8 | 1.7 | 2.9 |
| Fe | Ru | Os | 26 | 44 | 76 | 9.1 | 9.3 | 9.3 | 14.3 | 14.6 | 16.3 | 564 | 450 | 352 | 1.9 | 2.5 | 2.8 |
| Co | Rh | Ir | 27 | 45 | 77 | 10.1 | 9.5 | 11.2 | 14.5 | 13.6 | 16.9 | 552 | 432 | 358 | 1.9 | 2.3 | 2.9 |
| Ni | Pd | Pt | 28 | 46 | 78 | 6.6 | 4.7 | 2.3 | 10.4 | 7.6 | 5.8 | 473 | 323 | 213 | 1.4 | 1.4 | 1.1 |
| Cu | Ag | Au | 29 | 47 | 79 | 4.3 | 3.0 | 2.0 | 6.7 | 4.3 | 4.0 | 373 | 247 | 180 | 1.0 | 0.9 | 0.9 |
| Zn | Cd | Hg | 30 | 48 | 80 | U | 0.4 | U | U | 0.9 | U | U | 118 | U | U | 0.3 | U |

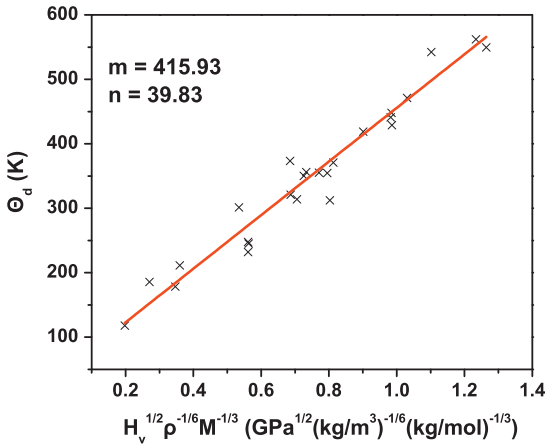


**Fig. 4.** Relationship between Debye temperature ($\theta_D$) from Eq. (9) versus hardness ($H_C$) from Eq. (8). Symbols are computed data points which have been shown only for mechanically stable structures of the anti-$ReO_3$ structured $M_3N$ compounds. A linear fit to Eq. (11), of Abrahams and Deus, is also shown.

where $m$ and $n$ are linear fitting coefficients. A plot depicting the relationship between Vickers hardness ($H_C$) and Debye temperature using the data obtained from the stable $M_3N$ compounds is shown in Fig. 4. By a linear fit to Eq. (11), we obtained $m$ = 415.93 K·(kg/m$^3$)$^{1/6}$ (kg/mol)$^{1/3}$/GPa$^{1/2}$ and $n$ = 39.83 K with a coefficient of determination of 0.951. These results indicate a relatively good fit and show that linearity between $\theta_D$ and $H_v$ is indeed followed in these anti-$ReO_3$ structured compounds, $M_3N$.

Moreover, $\theta_D$ can also be associated with melting point ($T_m$) using the equation given by Lindemann [57]:

$$T_m = b \times \theta_d^2 M V^{2/3}, \quad (12)$$

where $V$ is the unit cell volume corresponding to M, the molar mass of the unit cell, and $b$ is a linear fitting coefficient. Iso-structured materials with higher values of $H_V$ usually exhibit high melting points, due to higher bonding strength. Similar to high hardness, high melting point is also desired for hard coating materials, as it permits wider temperature range for their applications. The slope $b$ in Eq. (12), is unknown and therefore we can only compute ratios of the melting points ($T_m$) of different $M_3N$ compounds to the melting point of $Cu_3N$ in Kelvin. We chose $Cu_3N$ value of $T_m$ as the denominator, in the ratio, since it has been experimentally synthesized and we know its $T_m$ is above 740 K, the decomposition temperature of $Cu_3N$ [5,19]. The ratios so obtained are given in Table 3. The trend for $T_m$ is very similar to the trend for hardness. All $M_3N$ compounds exhibit higher melting points compared to $Cu_3N$, except for $Ta_3N$ and compounds of groups 1, 11, and 12. These values for $T_m$ correlate with their respective cohesive energies.

### 3.3. Electronic structure

We computed the electronic local density of states (LDOS) for all our $M_3N$ compounds. Some highlights of these results are now presented here. All the $M_3N$ compounds are found to be metallic due to the absence of any energy band gap around Fermi level ($E_F$), except for group 11, compounds, $Cu_3N$, $Ag_3N$ and $Au_3N$ with band gaps of about 0.17, 0.32 and 0.23 eV, respectively. It is well known that LDA systematically underestimates band gap by as much as 50% or more [58,59]. For small band gap materials it can even show metallic character, i.e. zero band gap. More accurate band gaps can be estimated using more advanced methods such as LDA+U, GW and others which are beyond the scope of the current work. Compounds we report as metallic may therefore possess small gaps if measured experimentally. Experimentally reported band gap of $Cu_3N$ has varied from about 0.8 to 1.9 eV, depending on variations in methods used and composition [60–62]. Our value of 0.17 eV is thus consistent with experimentally reported values for $Cu_3N$. Similar to the present work, earlier theoretical investigations on $Cu_3N$ have reported much smaller band gaps, varying from 0.169 eV to 0.40 eV varying by the computational method applied [40,63–66]. Although precise band gap values cannot be determined from LDA, it is clear that $Ag_3N$ and $Au_3N$ are likely to possess larger band gaps than $Cu_3N$ and act as semiconductors like $Cu_3N$.

Figs. 5–7 show plots of the LDOS as a function of energy for nitrides $M_3N$ of groups 7 ($Fe_3N$, $Ru_3N$ and $Os_3N$), 9 ($Ni_3N$, $Pd_3N$ and $Pt_3N$) and 12 ($Zn_3N$, $Cd_3N$ and $Au_3N$) respectively. For $M_3N$ compounds in the same column, it is seen that the electronic states spread wider and N 2 s orbital shifts lower as the atomic number goes up. Differences between LDOS plots of stable $M_3N$ compounds and unstable ones are distinctly observable. Figs. 5 and 6 show LDOS plots of $M_3N$ compounds with the largest bulk moduli (group

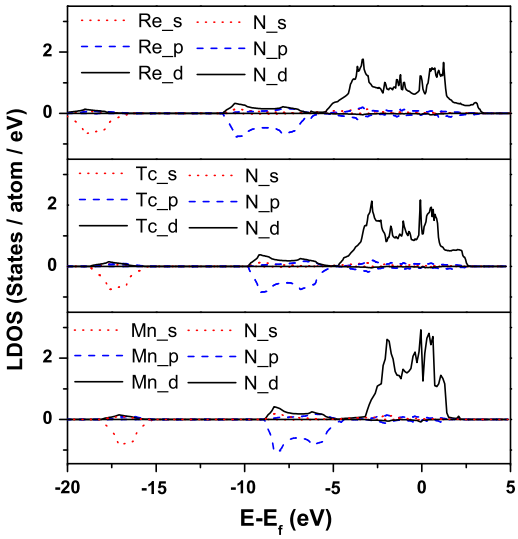


**Fig. 5.** Local density of states (LDOS) of nitrides, $Mn_3N$, $Tc_3N$ and $Re_3N$, with the highest values of $B$. Fermi energy is set to zero and LDOS corresponding to nitrogen sites have been denoted as negative values for clarity.

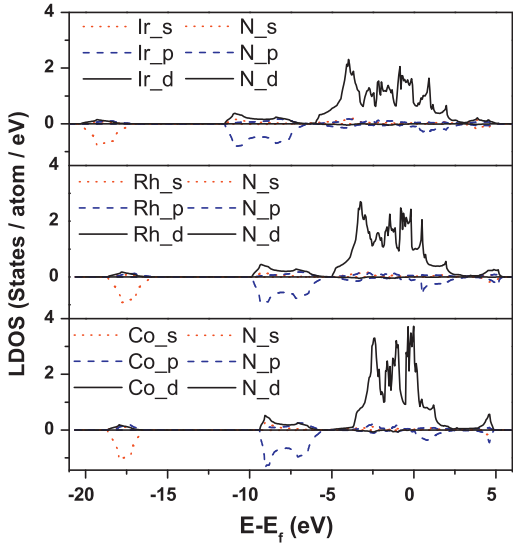


**Fig. 6.** Local density of states (LDOS) of nitrides, $Co_3N$, $Rh_3N$ and $Ir_3N$, with the highest values for $C_{44}$. Fermi energy is set to zero and LDOS corresponding to nitrogen sites have been denoted as negative values for clarity.

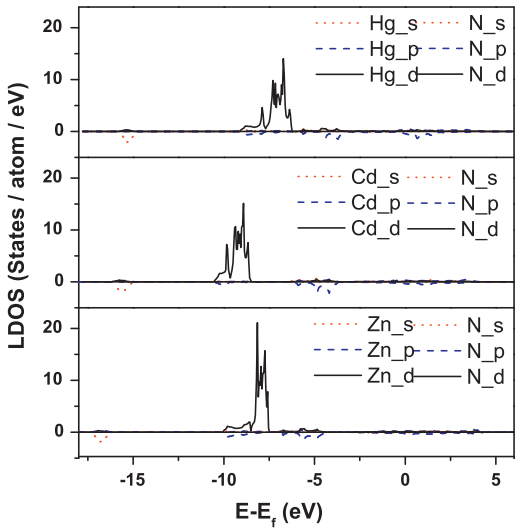


**Fig. 7.** Local density of states (LDOS) of nitrides, $Zn_3N$, $Cd_3N$ and $Hg_3N$, which are unstable or marginally stable. Fermi energy is set to zero and LDOS corresponding to nitrogen sites have been denoted as negative values for clarity.

7) and the greatest $C_{44}$ or hardness (group 9), respectively. For these very stable compounds, the metal d states are spread over a wide energy range below and above the Fermi energy and the LDOS varies smoothly with energy. In addition, these nitrides with higher $C_{44}$ values and hardness, exhibit strong hybridization of N 2*p* orbitals and metal *d* orbitals in the valence bands (below $E_F$). The relatively high hardness could be a result of high resistance to deformation forces due to strong $\sigma$ bonding between N 2*p* and metal d orbitals. We contrast these observations with the LDOS plot in Fig. 7 for group 12 $M_3N$ compounds which are generally unstable with $Cd_3M$ marginally stable, and their metal *d* electron states spread in relatively narrow energy ranges deep below their corresponding Fermi level. Their LDOS varies abruptly with energy. These results from Figs. 5–7 together with those of other nitrides, not shown, indicate the need for N 2*p* hybridization with the metal d states over a wide energy range for stability of the compounds to occur.

## 4. Conclusion

Transition metal nitrides with the anti-$ReO_3$ structure ($M_3N$) were investigated by density functional theory based calculations. Their lattice constants, energetic stability, electronic structure and mechanical properties including bulk modulus, Young's modulus, shear modulus, ductility, hardness, stability and Debye temperature are predicted. Narrow band gaps are found for group 11 $M_3N$ compounds, and the rest of the stable $M_3N$ compounds are metallic. Compounds of group 8 and 9 transition metals show relatively high hardness. Relation of metal *d* orbital hybridization with nitrogen 2*p* orbitals plays an important role in determining the stability of different compounds. Our work expands the database for nitrogen based coating materials and provides useful guidance for future experimental work. Such effort can now be navigated by focusing on materials of desired values for physical properties while avoiding efforts for synthesizing unstable compounds.

## Acknowledgments

The authors would like to thank the Ohio Supercomputer Center (OSC) and the National Science Foundation (NSF), through Grant No. CNS 0855134, for providing computing resources. We thank the Wright Center for PVIC of the State of Ohio and the University of Toledo as well as the NSF (Grants Nos. CMMI 1234777, CMMI 0928440, CMMI 0933069) for funding this work.

## Reference

[1] M. Hollek, J. Vac. Sci. Technol. A 4 (1986) 2661.
[2] S.-H. Jhi, J. Ihm, S.G. Louie, M.L. Cohen, Nat. Mater. 1 (2002) 19–25.
[3] A. Zerr, G. Miehe, R. Riedel, Nat. Mater. 2 (2003) 185–189.
[4] S. Kodambaka, S.V. Khare, V. Petrova, D.D. Johnson, I. Petrov, J.E. Greene, Phys. Rev. B 67 (2003) 035409.
[5] T. Maruyama, N. Morimoto, Appl. Phys. Lett. 69 (1996) 890–891.
[6] J. Perez-Rigueiro, C. Jimenez, J. Appl. Phys. 81 (1997) 781.
[7] E. Gregoryanz, C. Sanloup, M. Somayazulu, J. Badro, G. Fiquet, H.-k. Mao, R.J. Hemley, Nat. Mater. 3 (2004) 294–297.
[8] A.F. Young, C. Sanloup, E. Gregoryanz, S. Scandolo, R.J. Hemley, H.-k. Mao, Phys. Rev. Lett. 96 (2006) 155501.
[9] C.-Z. Fan, S.-Y. Zeng, L.-X. Li, Z.-J. Zhan, R.-P. Liu, W.-K. Wang, P. Zhang, Y.-G. Yao, Phys. Rev. B 74 (2006) 125118.
[10] R. Yu, X.F. Zhang, Phys. Rev. B 72 (2005) 054103.
[11] S.K.R. Patil, S.V. Khare, B.R. Tuttle, J.K. Bording, S. Kodambaka, Phys. Rev. B 73 (2006) 104118.
[12] J.C. Crowhurst, A.F. Goncharov, B. Sadigh, C.L. Evans, P.G. Morrall, J.L. Ferreira, A.J. Nelson, Science 311 (2006) 1275–1278.
[13] S.K.R. Patil, N.S. Mangale, S.V. Khare, S. Marsillac, Thin Solid Films 517 (2008) 824–827.
[14] W. Chen, J.Z. Jiang, J. Alloys Comp. 499 (2010) 243–254.
[15] E. Zhao, J. Wang, J. Meng, Z. Wu, Comput. Mater. Sci. 47 (2010) 1064–1071.
[16] E. Zhao, Z. Wu, J. Solid State Chem. 181 (2008) 2814–2827.
[17] Z.T.Y. Liu, X. Zhou, S.V. Khare, D. Gall, J. Phys. Condens. Matter 26 (2014) 025404.
[18] Z.T.Y. Liu, X. Zhou, D. Gall, S.V. Khare, Comput. Mater. Sci. 84 (2014) 365.
[19] R. Juza, H. Hahn, Z. Anorg. Allg. Chem. 239 (1938) 282–287.
[20] U. Zachwieja, H. Jacobs, J. Less-Common Metall. 161 (1990) 175–184.
[21] T. Maruyama, T. Morishita, J. Appl. Phys. 78 (1995) 4104–4107.
[22] J.G. Zhao, S.J. You, L.X. Yang, C.Q. Jin, Solid State Commun. 150 (2010) 1521–1524.
[23] J.A. Rodríguez M, M.G. Moreno-Armenta, N. Takeuchi, J. Alloys Comp. 576 (2013) 285–290.
[24] A. Wosylus, U. Schwarz, L. Akselrud, Matt G. Tucker, M. Hanfland, K. Rabia, C. Kuntscher, J. vonAppen, R. Dronskowski, D. Rau, R. Niewa, Z. Anorg. Allg. Chem. 635 (2009) 1959–1968.
[25] G. Kresse, in: Technische Universiät Wien, 1993.
[26] G. Kresse, J. Hafner, Phys. Rev. B 47 (1993) 558.
[27] G. Kresse, J. Furthmüller, Phys. Rev. B 54 (1996) 11169.
[28] P. Hohenberg, W. Kohn, Phys. Rev. 136 (1964) B864.
[29] W. Kohn, L.J. Sham, Phys. Rev. 137 (1965) 1697–1705.
[30] D. Vanderbilt, Phys. Rev. B 41 (1990) 7892.
[31] G. Kresse, J. Hafner, J. Phys. Condens. Matter 6 (1994) 8245–8257.
[32] H.J. Monkhorst, J.D. Pack, Phys. Rev. B 13 (1976) 5188.
[33] M.J. Mehl, J.E. Osburn, D.A. Papaconstantopoulos, B.M. Klein, Phys. Rev. B 41 (1990) 10311–10323.
[34] D.C. Wallace, Thermodynamics of Crystals, Wiley, New York, 1972.
[35] F. Birch, Phys. Rev. 71 (1947) 809–824.
[36] F.D. Murnaghan, Proc. Natl. Acad. Sci. USA 30 (1944) 244–247.
[37] J.P. Poirier, A. Tarantola, Phys. Earth Planet. Inter. 109 (1998) 1–8.
[38] H. Anton, P.C. Schmidt, Intermetallics 5 (1997) 449–465.
[39] W. Yu, J. Zhao, C. Jin, Phys. Rev. B 72 (2005) 214116.
[40] F. Kong, Y. Hu, Y. Wang, B. Wang, L. Tang, Comput. Mater. Sci. 65 (2012) 247–253.
[41] D.M. Teter, MRS Bull. 23 (1998) 6.
[42] X.-Q. Chen, H. Niu, D. Li, Y. Li, Intermetallics 19 (2011) 1275–1281.
[43] Y. Tian, B. Xu, Z. Zhao, Int. J. Refract. Metal. Hard Mater. 33 (2012) 93–106.
[44] M.K. Harbola, Proc. Natl. Acad. Sci. 89 (1992) 7.
[45] R. Hill, Proc. Phys. Soc. A 65 (1952) 5.
[46] W. Voigt, Lehrbuch der Kristallphysik, B.G. Teubner, Leipzig, Germany, 1928.
[47] A. Ruess, Z. Angew, Math. Mech. 9 (1929).
[48] D.H. Chung, W.R. Buessem, J. Appl. Phys. 38 (1967) 6.
[49] S.F. Pugh, Philos. Mag. Ser. 7 (45) (1954) 823–843.
[50] J. Haines, J. Léger, G. Bocquillon, Annu. Rev. Mater. Sci. 31 (2001) 1–23.
[51] D.G. Pettifor, Mater. Sci. Technol. 8 (1992) 345–349.
[52] O.L. Anderson, J. Phys. Chem. Solids 24 (1963) 909–917.
[53] F. Gao, J. He, E. Wu, S. Liu, D. Yu, D. Li, S. Zhang, Y. Tian, Phys. Rev. Lett. 91 (2003) 015502.
[54] P. Ravindran, L. Fast, P.A. Korzhavyl, B. Johansson, J. Wills, O. Eriksson, J. Appl. Phys. 84 (1998) 8.
[55] S.C. Abrahams, F.S.L. Hsu, J. Chem. Phys. 63 (1975) 4.
[56] P. Deus, H.A. Schneider, Cryst. Res. Technol. 18 (1983) 491–500.
[57] F.A. Lindemann, Phys. Z. 11 (1910) 4.
[58] M.C. Payne, M.P. Teter, D.C. Allan, T.A. Arias, J.D. Joannopoulos, Rev. Mod. Phys 64 (1992) 1045–1097.
[59] D. Medaboina, V. Gade, S.K.R. Patil, S.V. Khare, Phys. Rev. B 76 (2007) 205327.

[60] T. Nosaka, M. Yoshitake, A. Okamoto, S. Ogawa, Y. Nakayama, Appl. Surf. Sci. 169-170 (2001) 358–361.
[61] J.F. Pierson, Vacuum 66 (2002) 59–64.
[62] T. Nosaka, M. Yoshitake, A. Okamoto, S. Ogawa, Y. Nakayama, Thin Solid Films 348 (1999) 8–13.
[63] U. Hahn, W. Weber, Phys. Rev. B 53 (1996) 12684–12693.
[64] A. Soon, L. Wong, M. Lee, M. Todorova, B. Delley, C. Stampfl, Surf. Sci. 601 (2007) 4775–4785.
[65] M.G. Moreno-Armenta, A. Martínez-Ruiz, N. Takeuchi, Solid State Sci. 6 (2004) 9–14.
[66] Z.F. Hou, Solid State Sci. 10 (2008) 1651–1657.